Parametric investigation of pre-injection on the combustion, knocking and emissions behaviour of a large marine four-stroke dual-fuel engine

Huaiyu Wang[a,1], Huibing Gan[a,b,1*], Gerasimos Theotokatos[b]

[a] *Marine Engineering College, Dalian Maritime University, Dalian 116026, China*

[b] *Maritime Safety Research Centre, Department of Naval Architecture, Ocean and Marine Engineering, University of Strathclyde, 100 Montrose Street, Glasgow, G4 0LZ, Scotland, UK*

***Correspondence information:**

Huibing Gan

Marine Engineering College, Dalian Maritime University, Dalian 116026, China

E-mail address: ghbzq@dlmu.edu.cn

[1] **These authors contributed equally to this work.**

Nomenclature

DF:	Dual-fuel
CA:	Crank Angle
TDC:	Top Dead Center
BTDC:	Before Top Dead Center
ATDC:	After Top Dead Center
IMEP:	Indicated Mean Effective Pressure
HRR:	Heat Release Rate
THC :	Total Hydrocarbon
NO_X :	Nitrogen Oxide
1-D :	One-Dimensional
3-D:	Three-Dimensional
CFD:	Computational Fluid Dynamics
KI:	Knock Index
MP:	Monitoring Points
LNG:	Liquefied Natural Gas
IVC:	Intake Valve Closing
EVO:	Exhaust Valve Opening
SOI:	Start of Injection
SOPI :	Start of Pre-Injection
PMR:	Pre-Injection Mass Ratio
PMI:	Pre-Injection and Main Injection Interval
SOMI:	Start of Main Injection
MMR:	Main Injection Mass Ratio
PFP:	Peak Firing Pressure
PFPCA:	The Crank Angle of Peak Firing Pressure
THR:	Total Heat Release

DI : Direct Injection

FAT: Factory Acceptance Test

ASI: After Start of Injection

AMR: Adaptive Mech Refinement

IMO: International Maritime Organization

Abstract

This study aims at the parametric investigation of a large marine four-stroke dual-fuel engine in order to identify the pre-injection effects on the engine combustion, knocking and emissions parameters. A model was employed that was developed by integrating a 1-D engine model in AVL-BOOST and a 3-D CFD model in CONVERGE. The MAN 51/60DF marine engine is modelled and the simulation results were validated against experimental data. Subsequently, parametric runs for various pre-injection timings and mass ratios are performed and the simulation results are analysed and discussed. The derived in-cylinder pressure oscillations at determined points are employed to calculate the knock index (KI), which was used as an evaluation indicator for the knocking intensity. A number of pre-injection strategies with varying timing and fuel mass ratios are studied. This study results reveal that a lower knock trend and NO_X emissions can be achieved by early pre-injection timing and increasing pre-injection fuel mass ratio. In addition, the medium pre-injection interval increases the engine IMEP while reducing the NO_X and total hydrocarbon emissions. Larger pre-injection mass ratio reduce the KI and NO_X emissions, but reduces IMEP and causes the wetted-wall phenomenon. Besides, the excessive pre-injection intervals and pre-injection mass ratio result in a change in combustion mode from the conventional diesel compression ignition mode to a two-stage auto-ignition mode. This study provides a better understanding of the underlying interactions of involved parameters and proposes pre-injection solutions to improve the engine performance, emissions and knocking behaviour.

Keywords: Large marine DF engine; Pre-injection Strategies; Knocking; Combustion; Emissions

1. Introduction

The main power machinery is the diesel engine in the marine field, due to the advantages of high power, high efficiency, low energy consumption and high reliability [1]. At the same time, marine engines emit a wide variety of pollutants that have important impacts on health and climate change [2]. Policies and regulations to reduce nitrogen oxide (NO_X) emissions are strict, especially those rules aiming at exhaust emissions restriction of marine engines, which are major NO_X emissions sources [3]. In particular, the International Maritime Organization (IMO) has established specific emissions limitations for marine diesel NO_X pollutants [4]. IMO Tier III standard drastically limits the NOx emissions equal to 80 % of the Tier I standard [5]. Natural gas, which is the most used fossil fuel and the premium fuel of the twenty-first century, is desirable for various utilizations [6]. The use of liquefied natural gas (LNG) for ship propulsion reduces NO_X, SO_X emissions as its higher H/C ratio characteristic compared with diesel or heavy fuel oils [7]. The natural gas has a more attractive price advantage when taking the market fluctuations and fuel prices into account. Compared to other fossil fuels, natural gas is being developed at an ever-increasing rate in the world due to its environmental benefits [8]. Domestic natural gas supplies are increasing, and natural gas prices have remained lower than oil prices over the past decade [9]. Natural gas-diesel dual-fuel (DF) engines produce lower NO_X emissions when compared to conventional diesel engines [10]. The dual-fuel engine with low-pressure direct injection (DI) mode is a classical application mode, which retains the structure of the traditional engine to the greatest extent [11].

To improve the performance of dual-fuel engines, reduce emissions, and optimize the in-cylinder combustion process, the researchers have carried out relevant experimental and simulation studies [12-17]. The natural gas exhibits greater resistance to knocking due to its higher octane numbers (up to 120) and auto-ignition temperatures [18, 19]. However, the complex chemical kinetic characteristics of dual-fuel and the unique physical and chemical characteristics of natural gas lead to poor engine combustion stability, knock and other problems [20-23]. The experimental and simulation methods were adopted by many researchers, which are used to improve the performance of dual-fuel engines, reduce emissions, and optimize the in-cylinder combustion process [24]. Stoumpos et al. [25] investigated the effect of engine parameters on the performance of a large marine dual-fuel engine model by using one-dimensional (1-D) GT-Power. Considering the injection methods of two different fuels, the DF model was further developed. This study provided a solution for reducing CO_2 and NO_X emissions when considering engine operating limits simultaneously. Yousefi et al. [26] studied the effect of diesel injection timing dual-fuel combustion at low load through an experimental and numerical research. The results showed that the NO_X emissions first increased and then decreased, and the coefficient of variation of IMEP decreased with the advance of injection timing. Liu et al. [27] studied the ignition characteristics and pressure oscillation of a low-speed marine low-pressure DI natural gas dual-fuel engines. The numerical research showed that the amplitude of pressure oscillation increased with the later injection timing of the pilot fuel. Liu et al. [28] studied injection strategies on a low-speed marine low-pressure DI natural gas DF engines with a pre-chamber. Three factors were considered, including variable absolute injection timing, variable pilot fuel injection, and variable gas fuel injection. The results showed that the advanced gas fuel injection and retarded pilot fuel injection timings led to partially premixed gas burn, and further advanced or retarded timings resulted in a more partially premixed gas burn. In addition, the effects of pilot fuel mass and equivalence ratio on ignition / extinction and pressure oscillation were investigated by Liu et al. [29]. Yuan et al. [30] investigated the miller cycle and pre-injection on a low-speed marine high-pressure DI natural gas DF engines numerically. The results showed that, compared with the pre-injection mass ratio, the injection interval had little effect on the pressure oscillation, but the excessive injection interval affected the combustion stage. Valladolid et al. [31] conducted a numerical study on the effect of diesel pilot distribution on the ignition process of the DF medium-speed marine engine. They found that, the diesel injection pressure had a larger impact on NO_X for early injection timings than that for late injection timings. Xu et al. [32] experimentally studied the pre-injection strategy for pilot diesel compression ignition natural gas engines. The experimental results showed that the pre-injection timing reduced the ignition intensity which decreased the burning rate of the gas mixture and lowered NO_X emissions. Zhao et al. [33] experimentally studied the pre-injection strategy of a diesel/natural-gas DF engine, which was modified from a six-cylinder direct injection common rail diesel engine. The results showed that the ignition phase was controlled by the main injection, which avoided the worsen combustion stability caused by the inconsistent ignition phase.

Based on the briefly reviewed literature above, it is revealed that the injection strategy has great potential for reducing the knock tendency, improving engine performance, improving fuel economy, and reducing emissions [30, 32]. However, fewer studies have been conducted on the laws of influence of pre-injection parameters on knock, combustion and emissions, and methods to optimize pre-injection parameters, especially in the field of marine medium speed large-bore DF engine [31, 34]. Due to the large size of marine DF engines, it is difficult to carry out relevant experiments [27, 35, 36]. The numerical simulations have been widely accepted as the best way and partial alternative to the research of large marine engines [3, 37]. DF engines have a wider lambda window and lower propensity to knock at low loads, but with low thermal efficiency, and high levels of NO_X and total hydrocarbon emissions. Therefore, the objective of this work is to understand the effect of the pre-injection strategy on the knock, combustion and emissions in a large marine medium-speed DF engine at low load.

In this study, the process of in-cylinder combustion and pressure development of a DF engine at low load was studied by using a three-dimensional (3-D) numerical simulation method [38]. The pre-injection strategy was simulated for combustion stability and knock of a large marine DF engine by commercial CONVERGE code. The novel contributions of this work include: Firstly, the effect of the pre-injection strategy on the combustion mode was elaborated. Further, the conditions and criteria for the occurrence of knock phenomena were revealed. Moreover, the knock index was defined with reference to the gasoline engine and was used as an indicator for the evaluation of the pre-injection strategy. The effects of pre-injection timing and pre-injection quantity on knock, combustion and emissions were analyzed of a large marine DF engine at low load, which provided an important theoretical basis for the pre-injection strategy, improving the actual engine combustion stability, avoiding the phenomenon of knock, and improving engine combustion and emissions characteristics.

2. Modeling methodology

2.1. Investigated engine

The MAN 8L51/60 DF engine, which was a four-stroke, variable injection timing, turbocharged and intercooled DF engine, was used for the present study. The engine consists of eight cylinders placed in-line [39]. This type of engine is widely used due to its high power output, fuel flexibility, low emission rates, high efficiency and reliability. The natural gas is injected at each cylinder inlet port (upstream the intake valves) during the engine intake stroke. The pilot diesel fuel is injected directly into cylinders to ignite the gas mixture before top dead center. The engine details are reported in the manufacturer project guide [39] and factory acceptance test (FAT). The engine layout and components are presented in Fig. 1 [39]. The main particulars are listed in Table 1 [39].

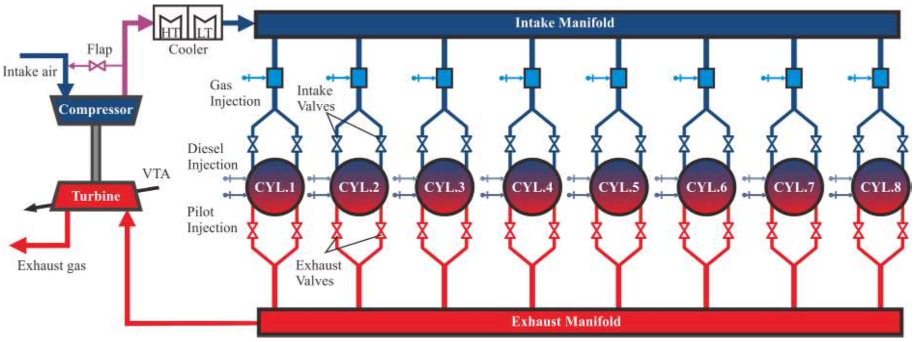

Fig. 1. Engine layout and components [39]

Table 1 MAN 8L51/60DF test engine specifications

Terms	Unit	Value
Cylinder number	[-]	8
Bore	[mm]	510
Stroke	[mm]	600
Compression ratio	[-]	13.3
Rated power	[kW]	8000
Rated speed	[r/min]	514
Mean effective pressure	[bar]	19.1
BSFC (Diesel model)	[g/kW·h]	189.1
BSEC (Gas model)	[kJ/kW·h]	7998
Turbocharger units	[-]	1
Fire order	[-]	1-4-7-6-8-5-2-3

2.2. Model set-up and calibration

In this paper, the combustion chamber geometry was modeled by using SolidWorks software. The Converge Studio was used to arrange the boundary, set calculation model and change calculation conditions. The CVG.in format data was the required files for Converge Solvers to calculate the combustion. The simulation working process coupled with 3-D calculation and 1-D coupling calculation is presented in Fig. 2. As can be seen from Fig. 2., the initial conditions of the 3-D model were provided by the 1-D model and the 1-D model was calibrated by the FAT [40].

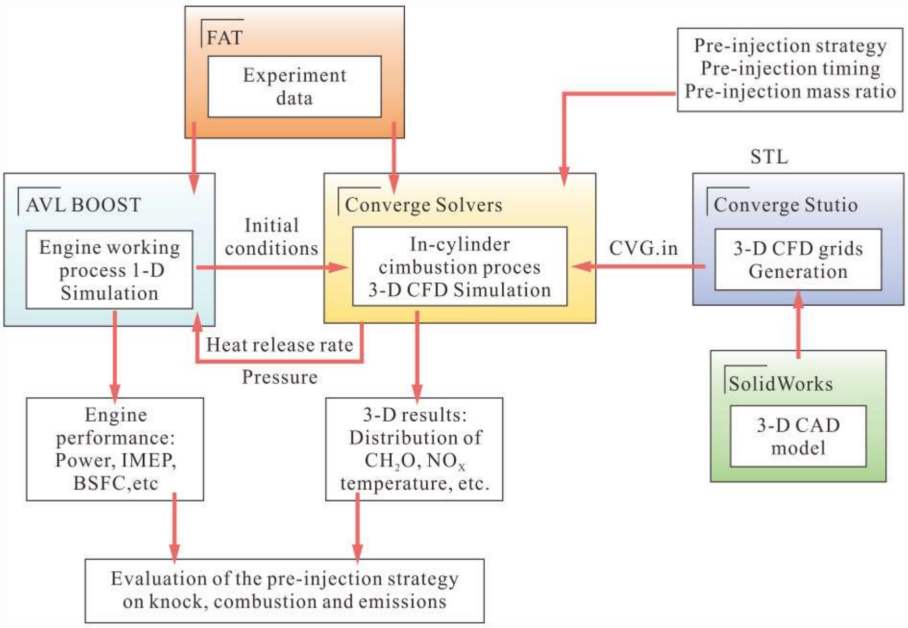

Fig. 2. Process of 3-D calculation and 1-D coupling calculation

2.2.2. 1-D simulation model calibration

In this study, the boundary conditions and initial conditions were provided by using AVL-BOOST [41], and in-cylinder combustion was calculated by using CONVERGE code [42]. The AVL-BOOST is widely used in 1-D simulation for engine modeling and analysis [41]. The DF engine mode in AVL-BOOST environment is presented in Fig. 3 [12]. The engine modeling and calibration were omitted here and the general method can be found in our previous works [12, 43]. The validation results of the primary parameters of DF engine model in the gas model are reported in Table 2 and Fig. 4 [12]. The parameters in Fig. 4 were normalized based on 75% load.

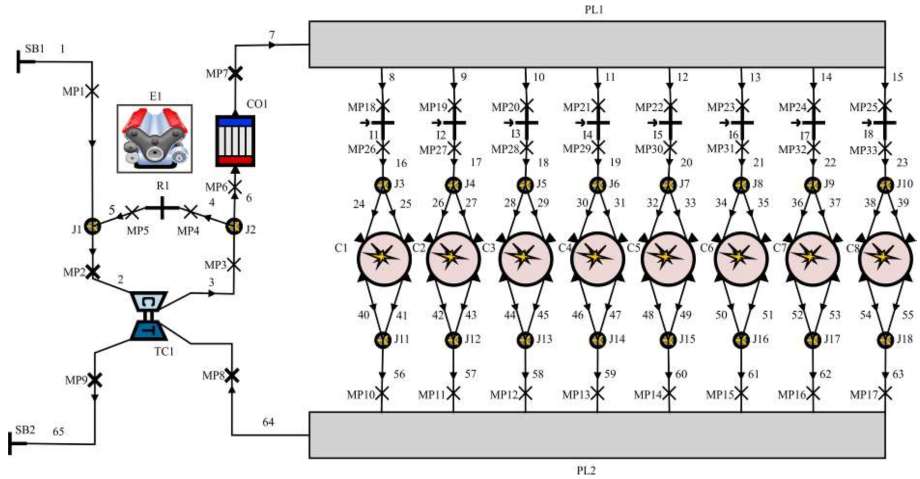

Fig. 3. Dual-fuel engine mode in AVL-BOOST environment [12]

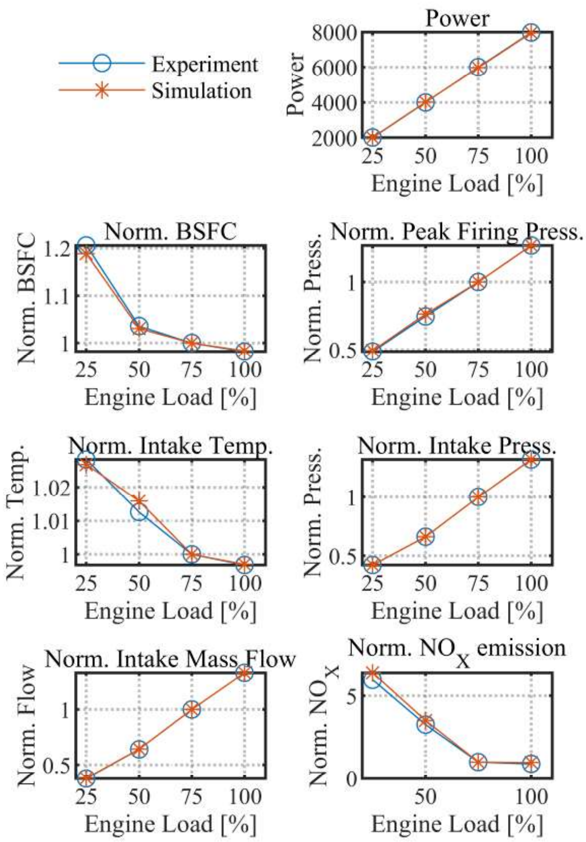

Fig. 4. Validation results of primary parameter of model [12]

Table 2 Validation results of primary parameter of model [12]

Engine Load [%]	100	75	50	25
Mode	Gas Mode Error (%)			
Power [kW]	0.12	0.14	-0.09	0.38
BSFC [g/kW·h]	-0.09	-0.11	0.13	-0.34
Peak Firing Pressure [bar]	-1.81	-1.72	0.44	0.51
Intake Manifold Temperature [K]	-0.99	-0.64	0.34	-2.00
Intake Manifold Pressure [bar]	-0.04	-0.24	-0.12	-0.11
Intake Manifold Mass Flow [kg/h]	-0.12	-0.22	0.16	0.67
Exhaust Manifold Temperature [K]	-1.98	0.27	0.10	2.79
Exhaust Manifold Pressure [bar]	1.28	2.59	2.23	-0.62
Exhaust Manifold Mass Flow [kg/h]	-0.16	0.14	-0.09	0.38
NO_X Emissions [g/kW·h]	1.59	-2.43	-1.96	1.98

2.2.3. 3-D simulation model calibration

In the CFD model, the marine engine numerical simulation also is based upon continuity, momentum and energy conservation laws [42, 44]. The compressible equations for mass transport, momentum transport and energy are given by Eqs. (1)-(3).

$$\frac{\partial \rho}{\partial t} + \frac{\partial \rho u_i}{\partial x_i} = S \qquad (1)$$

$$\frac{\partial \rho u_i}{\partial t} + \frac{\partial \rho u_i u_j}{\partial x_j} = -\frac{\partial P}{\partial x_i} + \frac{\partial \sigma_{ij}}{\partial x_j} + S_i \qquad (2)$$

$$\frac{\partial \rho e}{\partial t} + \frac{\partial u_j \rho e}{\partial x_j} = -P\frac{\partial u_j}{\partial x_j} + \sigma_{ij}\frac{\partial u_i}{\partial x_j} + \frac{\partial}{\partial x_j}\left(K\frac{\partial T}{\partial x_j}\right) + \frac{\partial}{\partial x_j}\left(\rho D \sum_m h_m \frac{\partial Y_m}{\partial x_j}\right) + S \qquad (3)$$

In the above equations, u is velocity, ρ is density, S is the source term, P is pressure, T is temperature, Y_m is the mass fraction of species m, D is the mass diffusion coefficient, e is the specific internal energy, K is the conductivity, h is the species enthalpy and σ_{ij} is the stress tensor [45].

In addition, each submodel needed to be determined, such as the turbulence model, combustion model, spray model, etc [46]. The DF engines with two different property fuels are complicated not only fluid flow, but also chemical reactions as well as heat and mass transfer. The suitable selection of models was required to simulate the dual-fuel engine. The Blob injection model [47] was implemented to simulate Liquid injection. The KH-RT model was applied to the simulation of spray breakup [48]. The Frossling model [49] was used as an Evaporation model. The O'Rourke and Amsden model [50] was used to calculate the wall heat transfer. Numerical simulation of RNG *k-ε* two-equation equation model coupled with a detailed chemical reaction had shown excellent simulation results in different types of fuels and engines [46, 51-55]. The various reaction mechanisms can be adapted in SAGE combustion model with a fast calculation [56]. As described by Turns [44], the mechanism of the multi-step chemical reaction can be described as Eqs. (4).

$$\sum_{m=1}^{M_{tot}} v'_{m,r}\,\chi_m \Leftrightarrow \sum_{m=1}^{M_{tot}} v''_{m,r}\,\chi_m \qquad r = 1,2\ldots\ldots R_{tot} \qquad (4)$$

where the $v'_{m,r}$ and $v''_{m,r}$ are the stoichiometric coefficients for the reactants and products, respectively, for species m and reaction r ; The R_{tot} represents the total number of the reactions; And the χ_m means the chemical symbol for species m .

The $\dot{\omega}_m$ represents the net production rate of species m and it can be described as Eqs. (5).

$$\dot{\omega}_m = \sum_{r=1}^{R_{tot}} v_{m,r} q_r \qquad \left(m = 1,2\ldots\ldots M_{tot}\right) \qquad (5)$$

where the M_{tot} is the total number of species.

The rate-of-progress parameter q_r for the r^{th} reaction is given by Eqs. (6).

$$q_r = k_{fr}\prod_{m=1}^{M_{tot}}\left[X_m\right]^{v'_{m,r}} - k_{rr}\prod_{m=1}^{M_{tot}}\left[X_m\right]^{v''_{m,r}} \qquad (6)$$

where the $\left[X_m\right]$ is the molar concentration of species m . The k_{fr} and k_{rr} are the forward and reverse rate coefficients for reaction r respectively.

With the above equation, the governing equation for mass is given by Eqs. (7).

$$\frac{d\left[X_m\right]}{dt} = \dot{\omega}_m \quad (7)$$

The governing equation for energy is given by Eqs. (8).

$$\frac{dT}{dt} = \frac{V\frac{dP}{dt} - \sum_m \left(\bar{h}_m \dot{\omega}_m\right)}{\sum_m \left([X_m]\bar{c}_{p,m}\right)} \qquad (8)$$

where the $\bar{h}_m$ and $\bar{c}_{p,m}$ are the molar specific enthalpy and molar constant-pressure specific heat of species m, respectively. The V, P and T are the volume, pressure and temperature, respectively. The above equations are solved at each computational time-step and the species are updated appropriately.

In order to obtain a more accurate model, the spray model was calibrated in this paper. The experimental data for calibration were obtained from Sandia National Laboratories [57, 58]. Sandia National Laboratories performed the high-fidelity parameter measurements of spray penetration, liquid length, vapor penetration, etc. in a constant-volume combustion vessel [57, 58]. The parameters of ambient and fuel injector conditions for calibration are listed in Table 3. Detailed experimental data can be found in the literature [58]

Table 3 Ambient and fuel injector conditions [58]

Terms	Unit	Value
Fuel type	[-]	*n*-heptane
Ambient temperature	[K]	1000
Ambient density	[kg/m^3]	14.8
Injection pressure	[MPa]	150
Fuel temperature	[K]	373
Nozzle diameter	[mm]	0.1
Injection duration	[ms]	6.8
Total mass injected	[mg]	17.8

The model used for calibration with the computational grid is presented in Fig. 5. As shown in Fig. 5, spray fixed embedding and adaptive mech refinement (AMR) were used for the numerical simulation. The diameter of the model is 108 mm and the height is 108 mm. The vaporizing diesel spray of experiments and simulation are presented in Fig. 6. The experiments (instantaneous) was the instantaneous measurements of vaporizing diesel spray by Rayleigh imaging. The experiments (mean) was the mean behavior of the diesel spray which was computed from the dataset. It can be seen from the Fig. 6 that the simulated penetration is almost consistent with the measured penetration, which shows the accuracy of the spray model setting. Fig. 7 shows the comparison of vapor penetration. It can be seen from the Fig. 7 that the simulation result at 0.8 ms is slightly smaller than the experiment. This is due to the limitation of the larger grid and the RNG k-ε model, resulting in the inability to capture vapor penetration well [57]. Where the ASI is after start of injection.

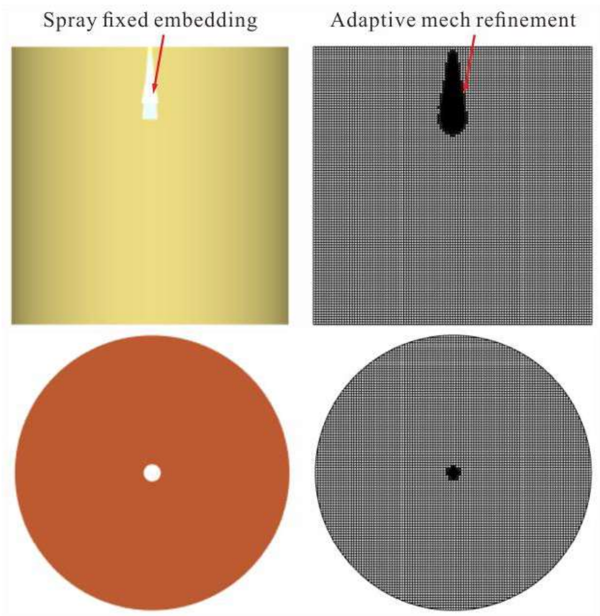

Fig. 5. Model and grid for diesel spray simulation

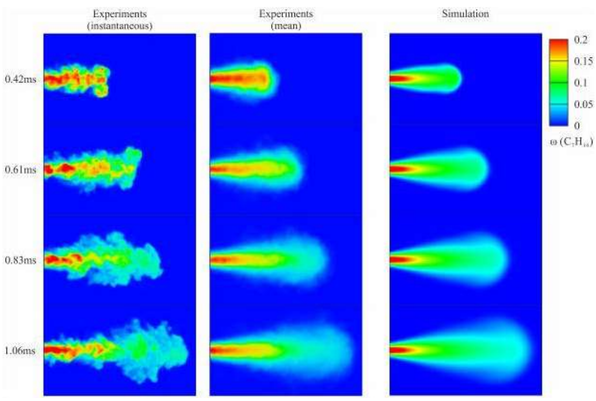

Fig. 6. Mixture fraction distributions

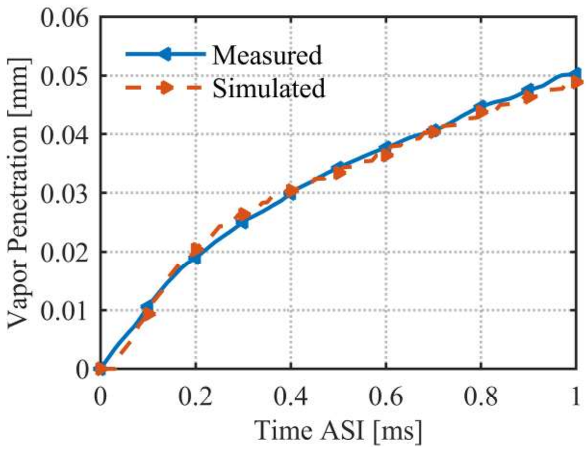

Fig. 7. Comparison of vapor penetration

In DF numerical studies, the methane and n-heptane are commonly used as alternative fuels for natural gas and diesel due to its similar physicochemical properties [29, 53]. The Extended Zeldovich NO_X mechanism was applied to simulate the production of NO_X [59]. The DF mechanisms which were developed by Rahimi, et al. [60] were obtained by merging n-heptane mechanisms and methane mechanisms. This combustion mechanism was widely used in the combustion of DF engines and made it possible to calculate cylinder pressure and NO_X emissions more accurately[28, 29, 61]. The selected mathematical models and chemical mechanisms are listed in Table 4. The combustion chamber geometry was modeled by using SolidWorks software and exported as an STL file, then imported into the CONVERGE software for boundary division [42]. The layout of the pilot injector with four holes in CONVERGE environment is presented in Fig. 8. As it is shown, the pilot injector is not located in the center of the cylinder, so the sector model cannot be used [39].

Table 4 Mathematical models and chemical mechanisms

Model	Setting
Turbulence	RNG k-ε model [49]
Spray breakup	KH-RT model [48]
Combustion	SAGE model [56]
NO_X formation	Extended Zeldovich model [59]
Reaction kinetics	Dual-fuel mechanism (GRI-Mech 3.0 and n-heptane) [60]

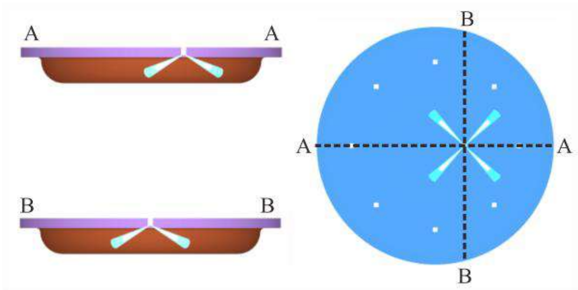

Fig. 8. The layout of pilot injector in CONVERGE environment

The grid control strategy in CONVERGE code is presented in Fig. 9. As it is shown, the grid control strategy includes a base value grid, adaptive mesh refinement, fixed embedding and grid scaling [42]. In this paper, the max embedding level and sub grid criterion of velocity adaptive mesh refinement were set to 2 layers and 2.0 m/s respectively. The max embedding level and sub grid criterion of temperature adaptive mesh refinement were set to 2 layers and 5.0 K respectively. The injection fixed embedding was set to 2 layers and the head and piston embedding is set to 1 layer. The grid scaling was usually used in compression stroke [29].

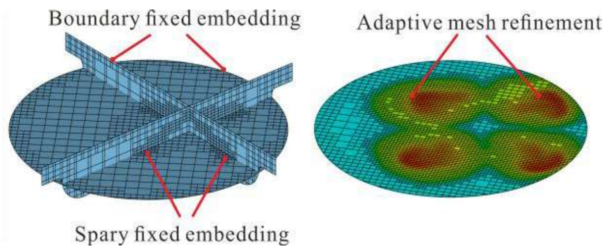

Fig. 9. Grid control strategy in CONVERGE code

The calculation time and calculation accuracy of CFD model were decided by mesh grid size [52]. To handle the relationship between time and accuracy, simulated in-cylinder pressures for 16, 20, and 24 mm base grids with grid control strategy were compared [62]. As it is shown in Fig. 10, the in-cylinder pressure trends of 16 and 20 mm are almost uniform and the in-cylinder pressure of 24 mm is lower than the 20 and 16 mm. Due to the large-bore and stroke of the engine, the small grid size causes the long calculation time. In this paper, the 20 mm base value grid was chosen to simulate the combustion process with the adaptive mesh refinement and fixed embedding grid control strategy [28, 63].

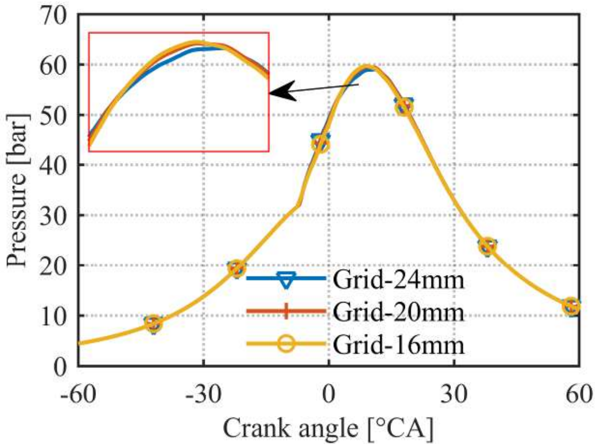

Fig. 10. Comparison of in-cylinder pressure curve with different basic grids

The peak firing pressure and emissions products were tested and used to validate the accuracy of the model. The 1-D simulation in-cylinder pressure curve was used to validate the 3-D simulation model. The 3-D engine simulation was performed by using the commercial CFD software package CONVERGE 2.4 [42]. The simulation started at IVC and ended at EVO, which means that only high pressure processes were simulated. The port fuel injected natural gas was considered to be homogeneously mixed with air at IVC [26]. The boundary, initial and operation conditions for the numerical simulation are illustrated in Table 5.

Table 5 Boundary, initial and operation conditions

Terms	Unit	Value
Boundary conditions		
Head	K	553
Piston	K	523
Wall	K	433
Initial conditions		
Temperature at IVC	K	355
Pressure at IVC	bar	1.12

Turbulent kinetic energy	m^2/s^2	40
Turbulent dissipation	m^2/s^3	1720
Operation conditions		
Load	[-]	25%
SOI	°BTDC	15
Speed	rpm	514

The engine speed was 514 r/min when operated at 25% load. The detailed parameters for modeling and calibrating are reported in Table 5. The in-cylinder pressure and emissions products were tested and used to validate the accuracy of the model. The comparison between the 3-D simulated and 1-D simulated in-cylinder pressure profiles and measured peak firing pressure (PFP) are presented in Fig. 11. The trend of the 3-D simulated results was in reasonable agreement with 1-D simulated results, but the 3-D calculated peak firing pressure is slightly lower than the measured results. In addition, the comparison of the key parameters between 3-D simulated and measured data are presented in Fig. 12. Where, the crank angle of peak firing pressure (PFPCA) and total heat release (THR) were compared with the 1-D simulated results and the PFP and NO_X were compared with the measured results. It can be inferred from Fig. 8. that the maximum errors between simulated results and measured data are within 2%. It can be concluded that the present model was capable of simulating the combustion process within the cylinder accurately.

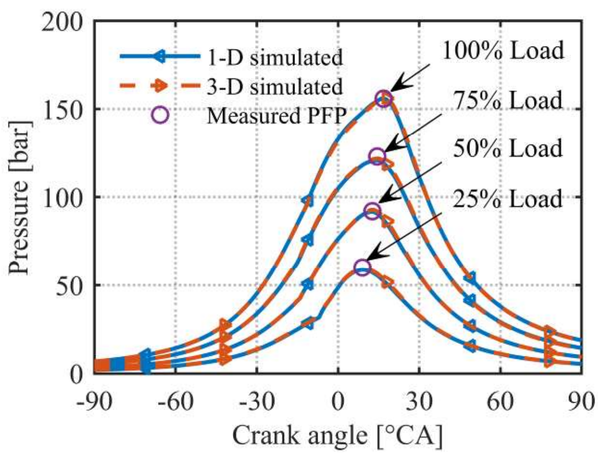

Fig. 11. Comparison between the 3-D simulated and 1-D simulated in-cylinder pressure profiles and

measured peak firing pressure

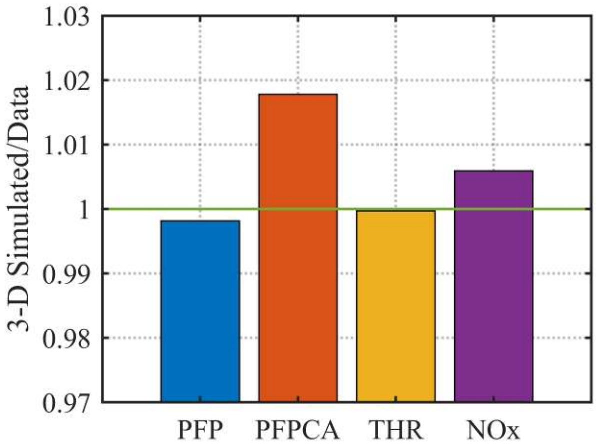

Fig. 12. Comparison of 3-D simulation and data values of key parameters

3. Pre-injection strategy and knock

3.1. Pre-injection strategy

The parameters defined for the pre-injection research are as follows. The SOPI is the start of pre-injection, the PMR is the pre-injection mass ratio, the PMI is the pre-injection and main injection interval, the SOMI is the start of the main injection and the MMR is the main injection mass ratio. The schematic diagram of the pre-injection parameters is illustrated in Fig. 13. It can be inferred from Fig. 13 that the PMI = SOPI - SOMI and the PMR = 1 - MMR.

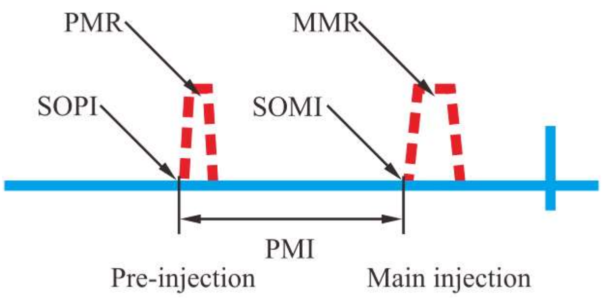

Fig. 13. Schematic diagram of pre-injection parameters

The parameters of the pre-injection strategy are shown in Table 6. It can be observed from Table 6 that Case 1 is the original single injection timing, Case 2 is the pre-injection timing strategy and Case 3 is the pre-injection mass ratio strategy.

Table 6 Parameters of the pre-injection strategy

Case	Load [%]	SOPI [deg ATDC]	PMR [-]	SOMI [deg ATDC]	MMR [-]	Step [deg or -]
1	25	—	—	-15	1.0	—
2	25	-20 ~ -60	0.5	-15	0.5	10
3	25	-60	0.1 ~ 0.9	-15	0.9 ~ 0.1	0.2

3.2. Pressure oscillation monitor and knock index

In order to monitor the pressure oscillations, the monitoring points (MP) were all placed near the wall of the combustion chamber and away from the injector, as shown in Fig. 14.

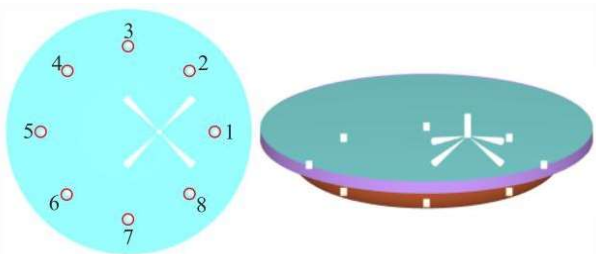

Fig. 14. Schematic diagram of monitoring points

In order to quantify the phenomenon of knock, the knock index (KI) was introduced to define the intensity of the knock [20, 46]. This parameter was defined as Eqs. (9).

$$KI = \frac{1}{N}\sum_{1}^{N} PP_{max,\, n} \qquad (9)$$

Where the $PP_{max,n}$ is the difference between the peak pressure at monitoring points and the peak in-cylinder pressure.

3.3. Analysis of cylinder pressure oscillation

In order to determine the limitation of KI, the knock of the original engine needs to be analyzed. The peak-to-peak values of each monitoring points are indicated in Fig. 15. It can be clearly seen from Fig. 15. that the pressure at monitoring points No. 1 and No. 8 are the largest, and the pressure at the monitoring point No. 2 is the smallest. The main reason for the dramatic change in pressure at monitoring point 8 is that the pilot injector is not located in the center of the combustion chamber, which cause the flame to spread different distances. It can be calculated that the knock index KI is 2.62 bar. So the maximum KI in this paper is limited to 2.62 bar.

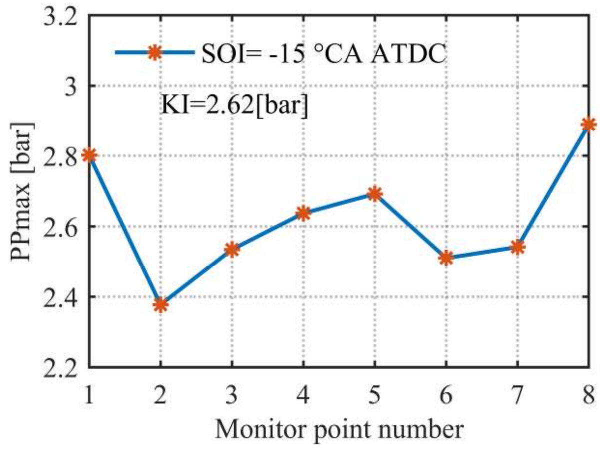

Fig. 15. Peak-to-peak pressure of the monitoring point and KI

4. Result and discussion

4.1. Knock analysis

Fig. 16 shows the KI in pre-injection. It can be seen in Fig. 16 (a) that the KI is lower than the base value when the SOPI = -30 and -50°CA, and the others SOPI are higher than the base value. The shorter injection interval causes KI to approach the base value at SOPI = -20 °CA. When the SOPI is after -30 °CA, the KI decreases as the SOPI is advanced. The KI increases when SOPI = -40 °CA and decreases when the injection interval continues to increase due to the change of the combustion mode. As can be seen from Fig. 16 (b), the KI changes very little when the pre-injection mass is relatively small, and is greatest when the pre-injection mass ratio is 0.5. This is because the combustion is controlled by the main injection fuel when the pre-injection mass ratio is small. The smaller pre-injection mass ratio equates to a slightly earlier injection timing, so the KI change is small. When the pre-injection mass ratio is 0.5, it results in unstable combustion because it is at the transition threshold of the combustion mode. When the pre-injection mass ratio is less than 0.5, the combustion is the traditional diesel compression ignition mode, when the pre-injection mass ratio is greater than 0.5, the combustion mode is the two-stage autoignition mode. However, when PMR is 0.9, the KI increases significantly because the temperature and pressure in the combustion chamber are lower during injection, and the injected fuel spreads around due to the swirl in the combustion chamber. This causes the combustion to start only after the main injection, resulting in a larger KI [15].

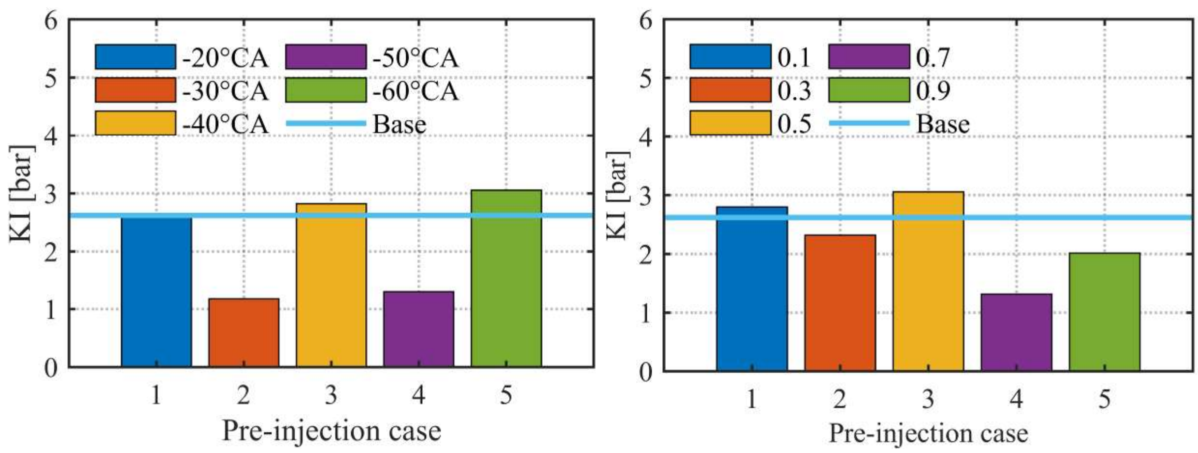

(a) KI with different SOPI

(b) KI different PMR

Fig. 16. Knock index

The pressure peak-to-peak value of each monitoring points with pre-injection is shown in Fig. 17. The points of polyline represent the maximum value of the pressure oscillation of each monitoring point. It can be seen in Fig. 17 that the pressure peak-to-peak values of the monitoring points No. 2 was higher than those of other monitoring points, indicating that the monitoring point of No. 6 is more prone to knocking. The close pressure difference indicates steady combustion and uniform pressure transfer.

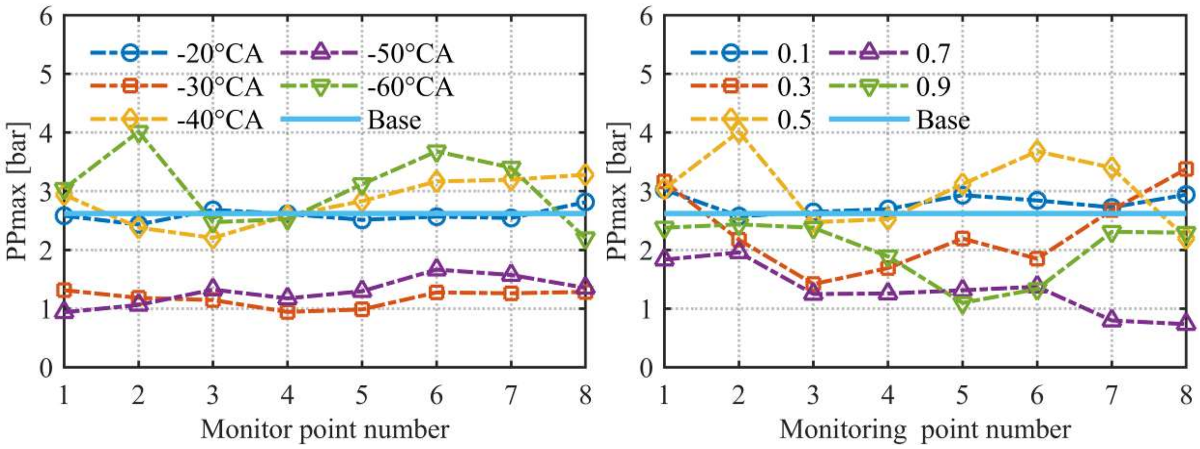

(a) PPmax with different SOPI (b) PPmax with different PMR

Fig. 17. Monitoring point pressure PPmax

For further understanding of the in-cylinder combustion processes, the distribution of the CH_2O radical is shown in Fig. 18. The white line in Fig. 18 is the 1800K temperature contour, which represents the flame front. The CH_2O is one of the most important intermediates in the CH_4 low temperature reaction, which is mainly distributed at the front of the flame, indicating that CH_2O is involved in the low temperature reaction [29]. The reaction rate of CH_2O directly influences the oxidation rate of methane, which affects the combustion process in the cylinder [61]. It can be seen from Fig. 18 (a) and (b) that when unstable combustion occurs, the distribution of CH_2O is far away from the 1800 K flame front. As can be seen from Fig. 18, the larger pre-injection interval to pre-injection mass ratio causes the fuel to adhere to the wall surface. This condition reduces KI, but causes the phenomenon of the wetted wall and limits the pre-injection strategy.

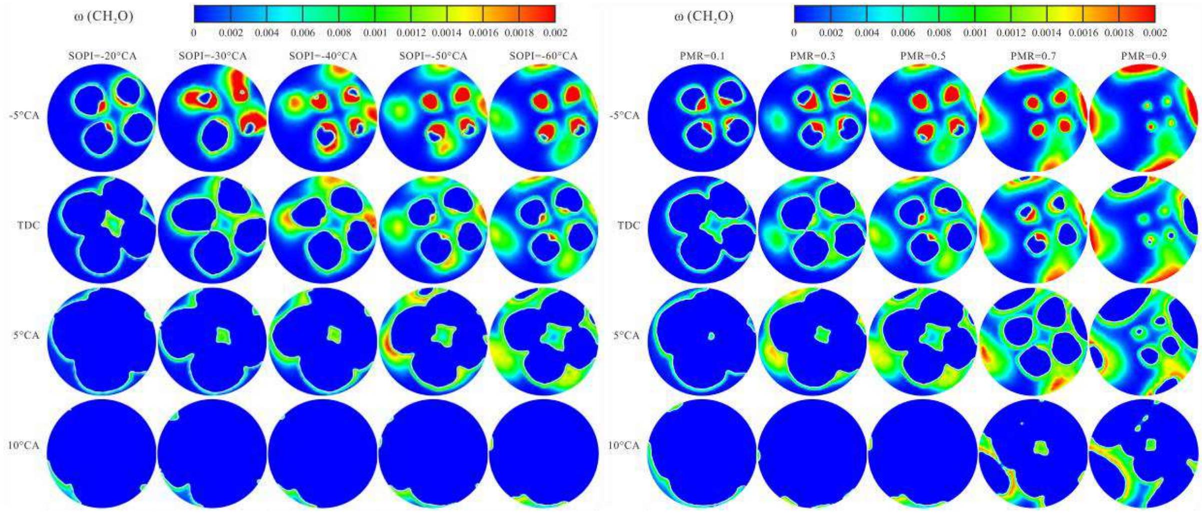

(a) CH_2O distribution with different SOPI (b) CH_2O distribution with different PMR

Fig. 18. In-cylinder CH_2O distribution with different SOPI

4.2. Combustion analysis

The variation of the in-cylinder pressure curve is presented in Fig. 19. As can be seen from Fig. 19 (a), the peak firing pressure decreases and then increases as the injection interval increases. The timing of the peak firing pressure is delayed by the increase in the injection interval. As can be seen from Fig. 19 (b), the peak firing pressure is greatest when the pre-injection mass ratio is 0.5. As the pre-injection mass ratio continues to increase, the cylinder pressure profile remains the same. This is because when the pre-injection mass is larger, the pressure and temperature of the chamber are lower during injection, resulting in weaker combustion control by the main injection, and the combustion mode changes to the two-stage autoignition mode.

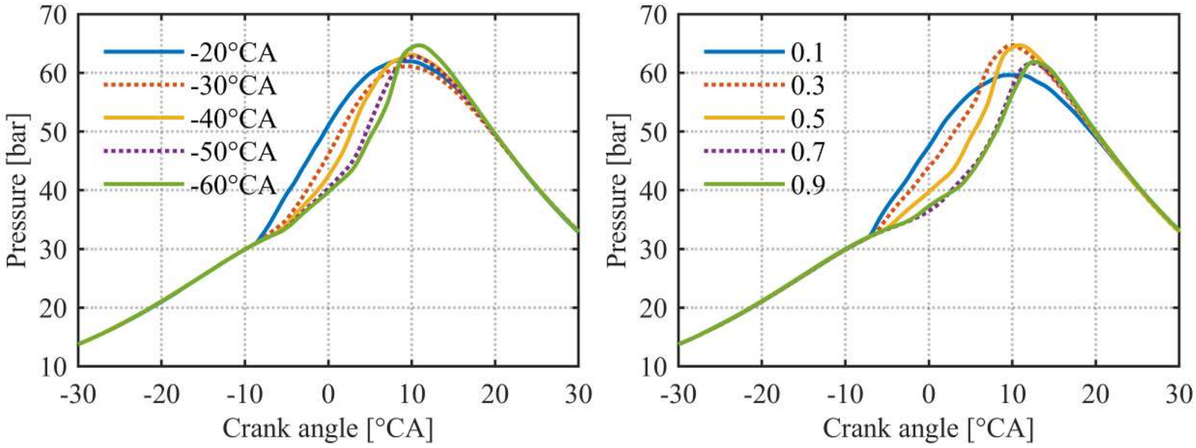

(a) Pressure curve with different SOPI (b) Pressure curve with different PMR

Fig. 19. In-cylinder pressure curve

Fig. 20 shows profiles of the heat release rate. It can be seen in Fig. 20 (a) that the advance of the SOPI leads to the increased peak in heat release rate (HRR) and causes the HRR curve to change from a single peak to twin peaks. Due to the complex combustion process of diesel-natural gas engines, the different physicochemical properties of diesel and natural gas result in a significant combustion time order of the two fuels [31]. When the injection interval is small (SOPI = -40~-30°CA), the advance pre-injection timing causes the first peak lower and the second peak higher. When the injection interval is large (SOPI = -60~-50°CA), the heat release rate shape becomes a single peak. As Fig. 20 (b) shows, the critical parameter for combustion mode transition is that the pre-injection mass ratio is 0.5, and when less than or greater than this ratio, the combustion beginning point is basically the same. The first peak is dominated by pre-mixed fuel and the second by the burnable gas mixture. When the pre-injection interval is large, the combustion chamber temperature and pressure during fuel injection are lower. This weakens the spraying and evaporating process of the fuel, allowing for increased periods of ignition delay [52]. However, when the pre-injection timing is too early (SOPI = -60°CA) and the pre-injection mass ratio > 0.5, the phenomenon of wetted wall occurs under the action of the in-cylinder swirl due to the low pressure in the combustion chamber and the long mixing time [26]. This causes the pre-injected fuel to burn near the wall surface and leads the unstable combustion [64, 65].

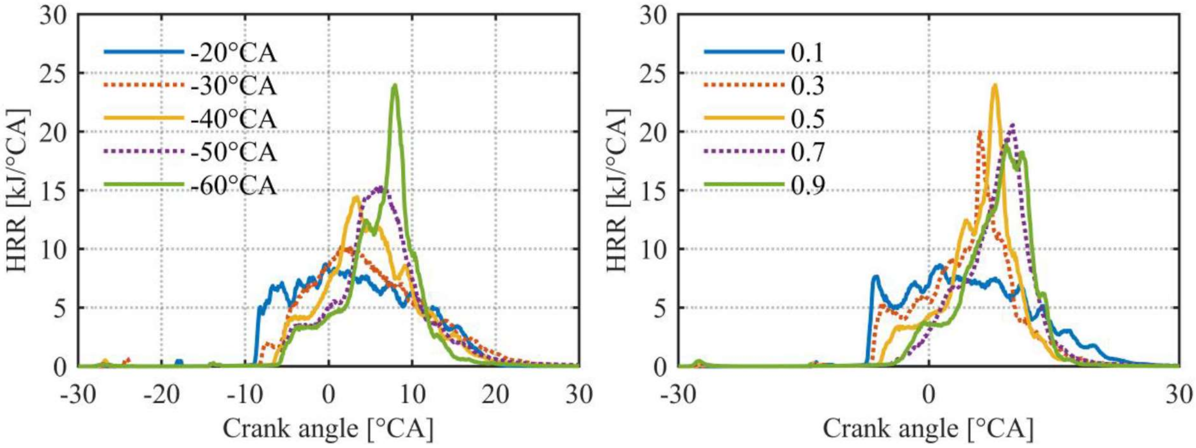

(a) HRR curve with different SOPI

(b) HRR curve with different PMR

Fig. 20. Heat release rate curve

Fig. 21 shows the variation of IMEP. It can be seen from Fig. 21 (a) that IMEP increases with the advance of SOPI. However, when SOPI is -60°CA, IMEP decreases. Fig. 21 (b) shows the IMEP with different PMR. It can be seen from Fig. 21 (b) that the IMEP is lowest at a pre-injection mass ratio of 0.1. The smaller pre-injection mass ratio is equivalent to slightly advancing the injection timing of a single injection, and the combustion is still controlled by the main injection, so the IMEP is smaller. IMEP is greatest when the pre-injection mass ratio is 0.3. This is because the large injection intervals allow for enough time for the fuel to mix. As the pre-injection mass ratio continues to increase, the main injection fuel control capacity decreases, causing the combustion phase to be delayed, which leads to a lower IMEP. This is because during fuel injection, the lower temperature and pressure of the combustion chamber with the longer mixing time results in the phenomenon of the wetted wall [51].

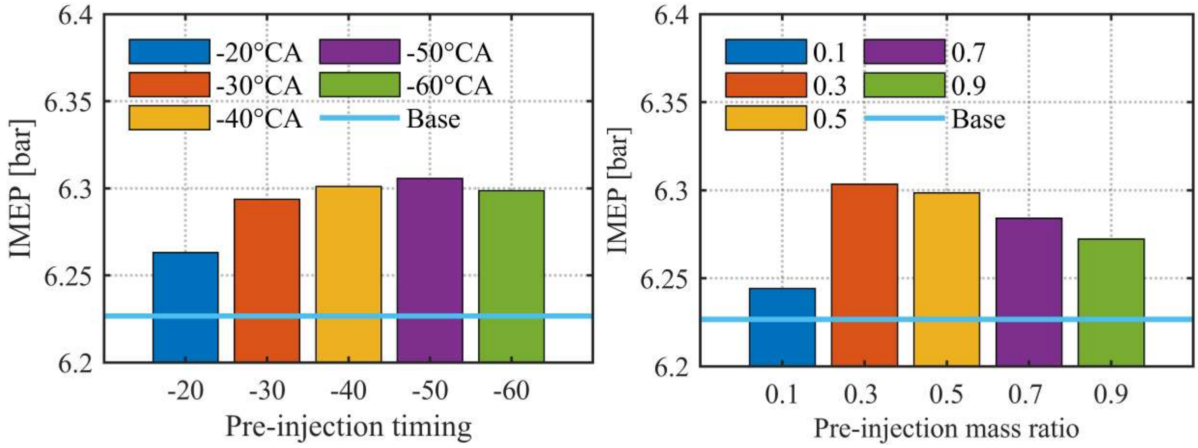

(a) IMEP with different SOPI (b) IMEP with different PMR

Fig. 21. Indicated mean effective pressure

4.3. Emissions analysis

The soot generation is higher in conventional diesels and smaller in dual-fuel engines, especially at higher rate of natural gas substitution [13, 15]. In this paper, the analysis focuses on NO_X, THC and CO emissions because of the high rate of natural gas substitution (> 95%).

Fig. 22 shows the comparison of indicated NO_X emissions. it can be seen from the Fig. 22 that at smaller pre-injection intervals (SOPI = -20 °CA), the advance of the injection timing leads to an increase in NO_X due to the larger injection ratio (PMR = 0.5), which is equivalent to the advance of the single injection timing. When a smaller pre-injection interval (SOPI = -20 °CA) is ignored, NO_X emissions are reduced by both increasing the pre-injection mass ratio and increasing the pre-injection interval. This is because the pre-injection strategy increases fuel mixing time, resulting in a wider distribution of fuel drip and lowering the maximum combustion temperature in the cylinder.

Fig. 23 shows the temperature distribution in the combustion chamber. The temperature profile provides a visual representation of the location of the high-temperature region in the combustion chamber and it is important for the analysis of NO_X emissions. The longer mixing time between the pre-injected diesel and natural gas mixture reduces the area of uneven local fuel concentration in the cylinder, which inhibits NO_X generation and thus reduces NO_X emissions. It can be seen from Fig. 23 that the high-temperature region decreases with increasing the pre-injection ratio and pre-injection interval when using the pre-injection strategy [53].

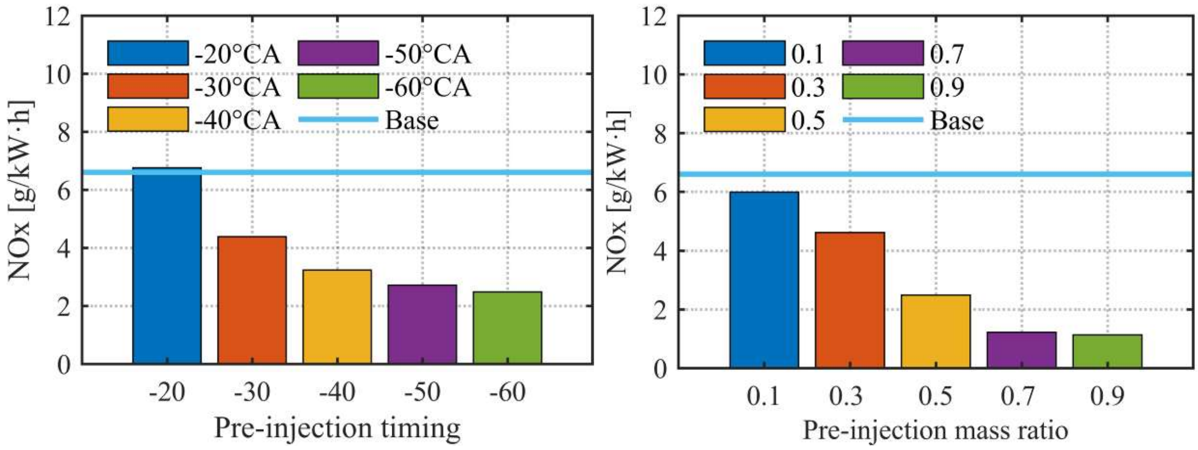

(a) NO_X emissions with different SOPI (b) NO_X emissions with different PMR

Fig. 22. Indicated NO_X emissions

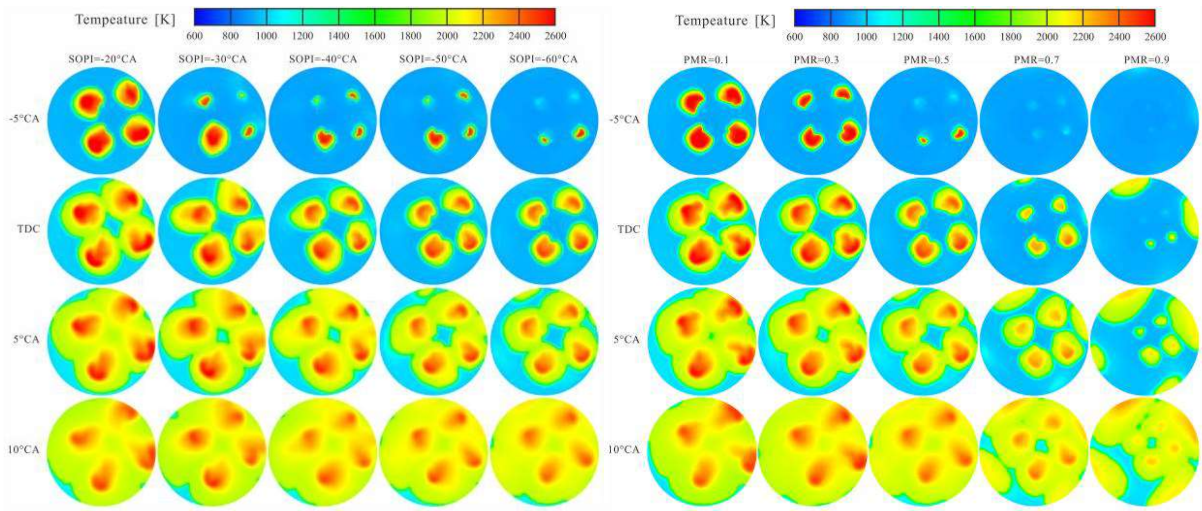

(a) Temperature distribution with different SOPI (b) Temperature distribution different PMR

Fig. 23. In-cylinder temperature distribution

The schematic diagram of temperature curve is presented in Fig. 24. As shown in Fig. 24, the temperature curve includes three curves which are mean temperature, maximum temperature and minimum temperature of the chamber. If the combustion chamber is divided into burned zone and unburned zone, the maximum temperature in Fig. 24 represents the temperature of the burned zone and the minimum temperature in Fig. 24 represents the temperature of unburned zone and the mean temperature represents the mean value of the in-cylinder temperature. According to previous studies, NO_X generation is mainly in the burned zone, so the burned zone temperature is particularly important for measuring NO_X generation [66]. The peak maximum temperature, peak mean temperature and peak minimum temperature are compared from Fig. 25. It can be seen from Fig. 25 that the peak maximum temperature decreases with increasing pre-injection interval and pre-injection mass ratio. The pre-injection interval has a significant effect on the peak maximum temperature, while the pre-injection mass ratio has a minor effect on the peak maximum temperature.

Fig. 26 shows the NO_X distribution in the combustion chamber. The local high combustion temperature regions are relatively wide which results in relatively higher NO_X emissions. As can be seen from Fig. 26, the NO_X distribution region in the combustion chamber is consistent with temperature, indicating that temperature is an important factor in the influence of NO_X. NO_X production is particularly small when the pre-injection mass ratio is large and pre-injection is positive [13].

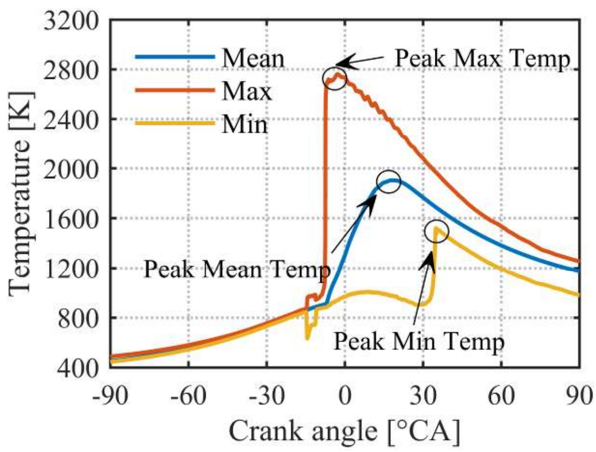

Fig. 24. Schematic diagram of temperature curve

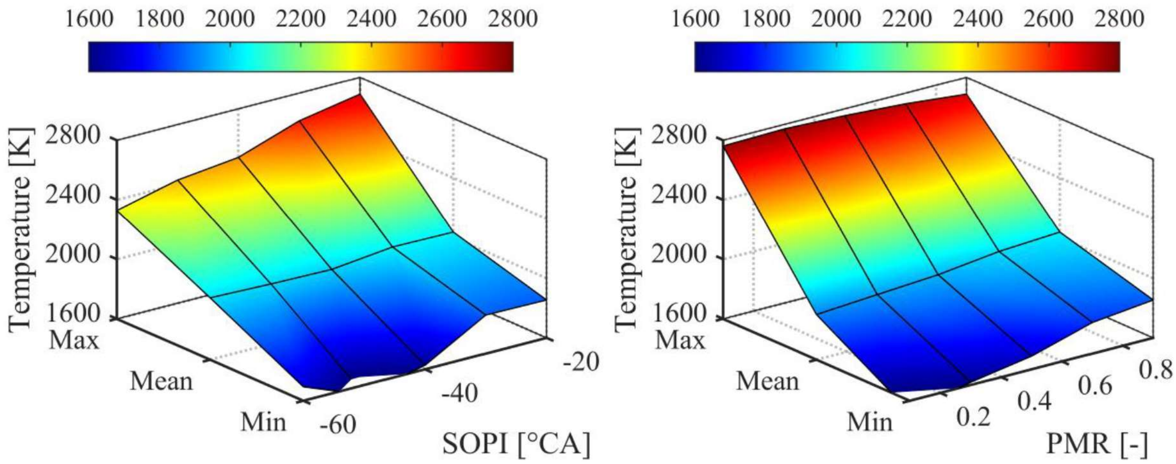

(a) Temperature comparison with different SOPI (b) Temperature comparison with different PMR

Fig. 25. Comparison of maximum temperature, average temperature and minimum temperature

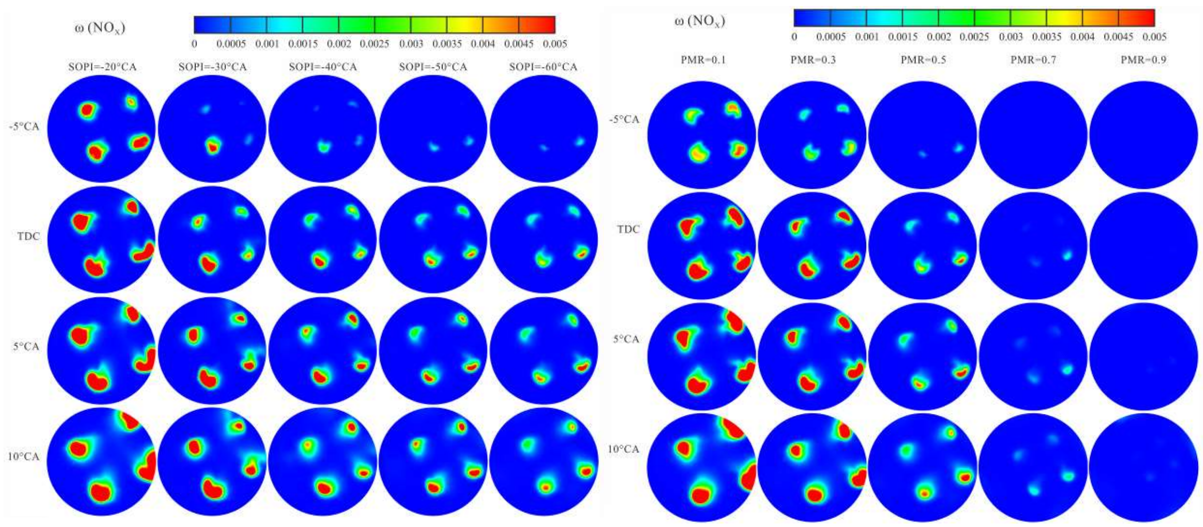

(a) NO_X distribution with different SOPI (b) NO_X distribution with different PMR

Fig. 26. In-cylinder NO_X distribution

The hydrocarbons is one of the main emissions of dual-fuel engines in ships, and in dual-fuel engines the main component of hydrocarbons is methane. Fig. 27 shows the mass change of total hydrocarbons (THC). As can be seen from Fig. 27, THC consumption is very slow before the TDC and rises sharply around 10 °CA with the pre-injection interval and pre-injection mass ratio increase. This is because at larger pre-injection intervals and pre-injection mass ratio, the injected fuel cannot burn immediately due to the lower temperature and pressure in the combustion chamber. Advancing pre-injection timing leads to leaner diesel and natural gas-air mixture formation which causes the combustion to start after the main fuel injection. When the pre-injection mass ratio is larger, the pre-injection fuel is distributed in the natural gas mixture. This promotes the production of flammable products in the middle of the flammable mixture, increasing the ignition area of the gas. The accelerated rate of combustion of the gas mixture has resulted in a higher utilization of natural gas. The combustion mode also transforms from the traditional diesel compression ignition mode to the two-stage autoignition mode [13].

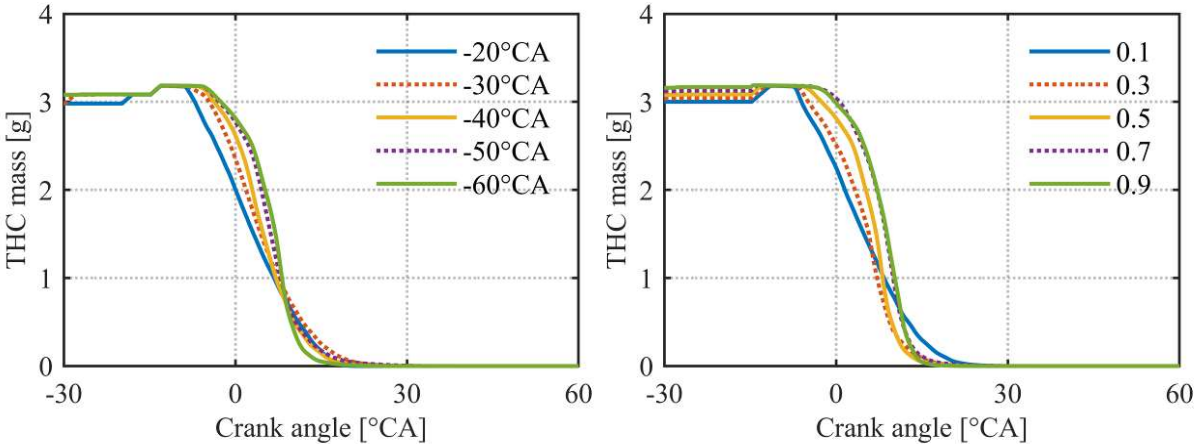

(a) THC change with different SOPI (b) THC change with different PMR

Fig. 27. Total hydrocarbon mass change

The changes of the CO are illustrated in the Fig. 28. It can be seen from Fig. 28. that compared to single injection mode, pre-injection considerably reduces the CO emissions. Further advancing pre-injection timing weakens the effect of pre-injected fuel on ignition and larger pre-injection mass and early pre-injection timing caused the longer mixture time for diesel and air which decreases the CO emissions.

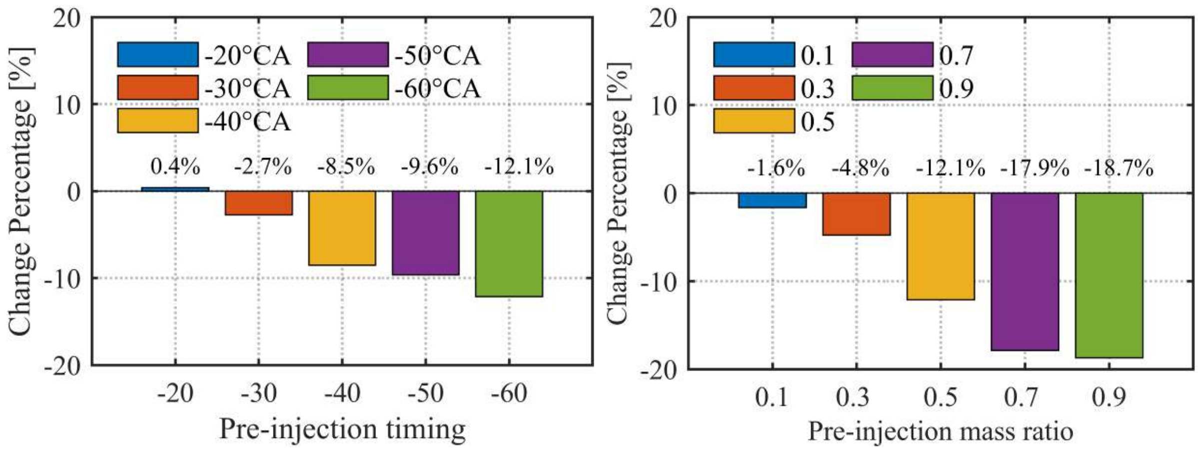

(a) CO change percentage with different SOPI　　(b) CO change percentage with different PMR

Fig. 28. CO change percentage comparison

5. Conclusions

In the present study, a large marine four-stroke DF engine was thoroughly investigated by using the CONVERGE software to reveal its knock, combustion and emissions chracteristics. The effects of pre-injection timing and pre-injection mass ratio on knock, combustion and emissions of the investigated engine has been studied numerically. The major concluding remarks from this study are summarized as follows.

1) The different combustion modes can be achieved by advancing the pre-injection time and increasing the pre-injection mass ratio. The critical parameters for the combustion mode transition were SOPI = -40°CA and PMR = 0.5, respectively. When the PMI > 25°CA and PMR > 0.5, the heat release rate shape becomes a single peak and the combustion phase shift backward.

2) When the KI is smaller, the difference between each measurement point is also smaller. KI decreases as the injection interval and pre-injection mass ratio increase when in the traditional diesel compression ignition mode, but reverses when in two-stage auto-ignition mode. When PMR = 0.5 and SPOI = -60°CA, the pressure difference at each measurement point is the largest and the KI is also the largest. The smallest KI can be obtained when the SOPI = -30 °CA and PMR=0.5, respectively.

3) The NO_X emissions decrease with increasing injection intervals and pre-injection mass ratio due to the longer fuel mixing time and lower maximum combustion temperature. The trend in CO emissions

is consistent with NO_X for different injection strategies. At PMR=0.5, the reduction in CO emissions becomes greater due to change of the combustion mode. The THC consumption accelerates with increasing injection intervals and pre-injection mass ratio, indicating that a proper pre-injection can reduce hydrocarbon emissions. However, when SOPI = -60 °CA, PMR = 0.7~0.9, the consumption rate is almost the same.

4) In all pre-injection strategies, IMEP is higher than a single injection. The IMEP increases with increasing pre-injection interval and decreases with increasing pre-injection mass ratio when large pre-injection intervals and small pre-injection mass ratio are not considered. The maximum can be achieved when the PMR = 0.5 and the SOPI = -50 °CA or the PMR = 0.3 and the SOPI = -60°CA.

5) Among the calculated cases, when NO_X, KI and IMEP are considered together, the best pre-injection parameters are SOPI = -50 °CA and PMR = 0.5. When considering KI alone, the lowest KI can be obtained when SOPI = -60°CA and PMR = 0.7. It can be reasonably estimated the best parameters are SOPI = -50 °CA and PMR = 0.3 when the goal is to reduce NO_X emissions without sacrificing economy and dynamics, and consider the limitation of KI and phenomenon of the wetted wall.

In conclusion, the present study provides the basis for the pre-injection strategy of DF engines and the results contributed to the better understanding the improvement of knocking, combustion and emissions by pre-injection strategy. The law of influence of the pre-injection strategy on the phenomenon of knock is explained, and a method for determining the phenomenon of knock is determined, which is also applicable to the determination of the phenomenon of knock of DF engines at high load. The current investigation helps to get a better understanding of the theoretical basis for the pre-injection strategy, improving the actual engine combustion stability, and avoiding the phenomenon of knock of the DF engines. In future work, machine learning algorithms will be used to model pre-injection strategies, and genetic algorithms will be combined with machine learning models to optimize pre-injection parameters.

Acknowledgements

This work was supported by the China Scholarship Council (grant number 201903210012); and the Fundamental Research Funds for the Central Universities (grant number 3132019315).

References

[1] Yoo B-Y. Economic assessment of liquefied natural gas (LNG) as a marine fuel for CO2 carriers compared to marine gas oil (MGO). Energy 2017;121(1):772-80.

[2] Tang Y, Zhang J, Jia B, He Z, Xia Y. Investigation on the solution of nitric oxide emission model for diesel engine using optimization algorithms. Fuel 2018;228(1):81-91.

[3] Jiang X, Wei H, Zhou L, Chen R. Numerical Study on the Effects of Multiple-Injection Coupled with EGR on Combustion and NOx Emissions in a Marine Diesel Engine. Energy Procedia 2019;158:4429-34.

[4] Späth N. DNV GL releases updated DNV GL NOx TIER III compliance guide; Available from: https://www.dnvgl.com/news/dnv-gl-releases-updated-dnv-gl-nox-tier-iii-compliance-guide-98168. [Accessed 2019-12-11.

[5] Troberg M, Delneri D. Tier III emission roadmap for marine engine application. MTZ worldwide 2010;71(6):12-7.

[6] Yousefi A, Birouk M. An Investigation of Multi-Injection Strategies for a Dual-Fuel Pilot Diesel Ignition Engine at Low Load. Journal of Energy Resources Technology 2016;139(1):012201--15.

[7] Burel F, Taccani R, Zuliani N. Improving sustainability of maritime transport through utilization of Liquefied Natural Gas (LNG) for propulsion. Energy 2013;57(1):412-20.

[8] Wik C, Niemi S. Low emission engine technologies for future tier 3 legislations - options and case studies. Journal of Shipping and Trade 2016;1(1):1-22.

[9] Takasaki K. Observations on the Development and Practical Application of Marine Gas Engines. ClassNK technical bulletin 2012;30:1-9.

[10] Maurya RK, Mishra P. Parametric investigation on combustion and emissions characteristics of a dual fuel (natural gas port injection and diesel pilot injection) engine using 0-D SRM and 3D CFD approach. Fuel 2017;210:900-13.

[11] Li G, Long Y, Zhang Z, Liang J, Zhang X, Zhang X, et al. Performance and emissions characteristics of a lean-burn marine natural gas engine with the addition of hydrogen-rich reformate. Int J Hydrogen Energ 2019;44(59):31544-56.

[12] Wang H, Gan H, Wang G, Zhong G. Emission and Performance Optimization of Marine Four-Stroke Dual-Fuel Engine Based on Response Surface Methodology. Math Probl Eng 2020;2020.

[13] Wang Z, Zhao Z, Wang D, Tan M, Han Y, Liu Z, et al. Impact of pilot diesel ignition mode on combustion and emissions characteristics of a diesel/natural gas dual fuel heavy-duty engine. Fuel 2016;167:248-56.

[14] Yang B, Ning L, Chen W, Wang B, Zeng K, Dong W. Parametric investigation the particle number and mass distributions characteristics in a diesel/natural gas dual-fuel engine. Appl Therm Eng 2017;127(1):402-8.

[15] Yousefi A, Guo H, Birouk M. An experimental and numerical study on diesel injection split of a natural gas/diesel dual-fuel engine at a low engine load. Fuel 2018;212(1):332-46.

[16] Zang R, Yao C. Numerical Study of Combustion and Emission Characteristics of a Diesel/Methanol Dual Fuel (DMDF) Engine. Energ Fuel 2015;29(6):3963-71.

[17] Zhou F, Fu J, Li D, Liu J, Lee C-fF, Yin Y. Experimental study on combustion, emissions and thermal balance of high compression ratio engine fueled with liquefied methane gas. Appl Therm Eng 2019;161:114125.

[18] Duan X, Liu J, Yao J, Chen Z, Wu C, Chen C, et al. Performance, combustion and knock assessment of a high compression ratio and lean-burn heavy-duty spark-ignition engine fuelled with n-butane and liquefied methane gas blend. Energy 2018;158:256-68.

[19] Duan X, Liu Y, Lai M-C, Guo G, Liu J, Chen Z, et al. Effects of natural gas composition and compression ratio on the thermodynamic and combustion characteristics of a heavy-duty lean-burn SI engine fueled with liquefied natural gas. Fuel 2019;254:115733.

[20] Lounici MS, Benbellil MA, Loubar K, Niculescu DC, Tazerout M. Knock characterization and development of a new knock indicator for dual-fuel engines. Energy 2017;141:2351-61.

[21] Maghbouli A, Shafee S, Saray RK, Yang W, Hosseini V, An H. A multi-dimensional CFD-chemical kinetics approach in detection and reduction of knocking combustion in diesel-natural gas dual-fuel engines using local heat release analysis. SAE International Journal of Engines 2013;6(2):777-87.

[22] Sremec M, Taritaš I, Sjerić M, Kozarac D. Numerical investigation of injection timing influence on fuel slip and influence of compression ratio on knock occurrence in conventional dual fuel engine. Journal of Sustainable Development of Energy, Water and Environment Systems 2017;5(4):518-32.

[23] Kirsten M, Pirker G, Redtenbacher C, Wimmer A, Chmela F. Advanced knock detection for diesel/natural gas engine operation. SAE International Journal of Engines 2016;9(3):1571-83.

[24] Mavrelos C, Theotokatos G. Numerical investigation of a premixed combustion large marine two-stroke dual fuel engine for optimising engine settings via parametric runs. Energ Convers Manage 2018;160:48-59.

[25] Stoumpos S, Theotokatos G, Boulougouris E, Vassalos D, Lazakis I, Livanos G. Marine dual fuel engine modelling and parametric investigation of engine settings effect on performance-emissions trade-offs. Ocean Eng 2018;157:376-86.

[26] Yousefi A, Birouk M, Guo H. An experimental and numerical study of the effect of diesel injection timing on natural gas/diesel dual-fuel combustion at low load. Fuel 2017;203:642-57.

[27] Liu C, Liu Z, Liu B, Zhou L, Wei H. Effect of Pilot Fuel Injection Timing on Ignition Characteristics and Pressure Oscillation in Natural Gas/Diesel Dual Fuel Engine. Journal of Tianjin University (Science and Technology) 2020;53(02):154-61.

[28] Liu H, Li J, Wang J, Wu C, Liu B, Dong J, et al. Effects of injection strategies on low-speed marine engines using the dual fuel of high-pressure direct-injection natural gas and diesel. Energy Science & Engineering 2019;7(5):1994-2010.

[29] Liu Z, Zhou L, Liu B, Zhao W, Wei H. Effects of equivalence ratio and pilot fuel mass on ignition/extinction and pressure oscillation in a methane/diesel engine with pre-chamber. Appl Therm Eng 2019;158:113777.

[30] Yuan C, Liu B, Jiang X, Zhou L, Chen R, Wei H. Numerical study on pressure oscillation suppression of low-speed marine engine with in-cylinder direct injection of natural gas. Chinese Internal Combustion Engine Engineering 2019;40(6):56-63.

[31] Valladolid PG, Tunestål P, Monsalve-Serrano J, García A, Hyvönen J. Impact of diesel pilot distribution on the ignition process of a dual fuel medium speed marine engine. Energ Convers Manage 2017;149:192-205.

[32] Xu M, Cheng W, Li Z, Zhang H, An T, Meng Z. Pre-injection strategy for pilot diesel compression ignition natural gas engine. Appl Energ 2016;179:1185-93.

[33] Zhao G, Jia Q, Yao C, Song E, Lu C, Sun J. Effect of Pre-Injection Strategy on Combustion and Emission Characteristics of Dual-Fuel Engines. Transactions of CSICE 2020(01):19-26.

[34] Gharehghani A, Mirsalim S, Jazayeri S. Numerical and experimental investigation of combustion and knock in a dual fuel gas/diesel compression ignition engine. Journal of Combustion 2012;2012.
[35] Baldi F, Theotokatos G, Andersson K. Development of a combined mean value–zero dimensional model and application for a large marine four-stroke Diesel engine simulation. Appl Energ 2015;154:402-15.
[36] He S, Du B-G, Feng L-Y, Fu Y, Cui J-C, Long W-Q. A Numerical Study on Combustion and Emission Characteristics of a Medium-Speed Diesel Engine Using In-Cylinder Cleaning Technologies. Energies 2015;8(5):4118-37.
[37] Li M, Zhang Q, Li G, Li P. Effects of Hydrogen Addition on the Performance of a Pilot-Ignition Direct-Injection Natural Gas Engine: A Numerical Study. Energ Fuel 2017;31(4):4407-23.
[38] Hockett A, Hampson G, Marchese AJ. Development and Validation of a Reduced Chemical Kinetic Mechanism for Computational Fluid Dynamics Simulations of Natural Gas/Diesel Dual-Fuel Engines. Energ Fuel 2016;30(3):2414-27.
[39] Turbo MD. 51/60DF Project Guide - Marine: Four-stroke dual-fuel engines compliant with IMO Tier II / IMO Tier III. MAN Diesel & Turbo; 2015.
[40] Feng L, Tian J, Long W, Gong W, Du B, Li D, et al. Decreasing NOx of a Low-Speed Two-Stroke Marine Diesel Engine by Using In-Cylinder Emission Control Measures. Energies 2016;9(4):304.
[41] GmbH AL. AVL BOOST Users Guide. 2016.
[42] Senecal P, Richards K, Pomraning E. CONVERGE (Version 2.4) Manual. *Convergent Science Inc., Madison, WI.* 2018.
[43] Gan H, Wang H, Tang Y, Wang G. Investigation of the Miller cycle on the performance and emission in a natural gas-diesel dual-fuel marine engine by using two zone combustion model. Therm Sci 2020;24(1 Part A):259-70.
[44] Turns SR. Introduction to combustion. New York: McGraw-Hill Companies; 1996.
[45] Shi C, Ji C, Wang S, Yang J, Ma Z, Xu P. Assessment of spark-energy allocation and ignition environment on lean combustion in a twin-plug Wankel engine. Energ Convers Manage 2020;209:112597.
[46] Li A, Zheng Z, Peng T. Effect of water injection on the knock, combustion, and emissions of a direct injection gasoline engine. Fuel 2020;268:117376.

[47] Reitz RD, Diwakar R. Structure of high-pressure fuel sprays. SAE transactions 1987:492-509.
[48] Beale JC, Reitz RD. Modeling spray atomization with the Kelvin-Helmholtz/Rayleigh-Taylor hybrid model. Atomization Spray 1999;9(6):623-50.
[49] Han Z, Reitz RD. Turbulence Modeling of Internal Combustion Engines Using RNG κ-ε Models. Combust Sci Technol 1995;106(4-6):267-95.
[50] Amsden AA, Findley M. KIVA-3V: A block-structured KIVA program for engines with vertical or canted valves. 1997.
[51] Nazemi M, Shahbakhti M. Modeling and analysis of fuel injection parameters for combustion and performance of an RCCI engine. Appl Energ 2016;165:135-50.
[52] Yousefi A, Guo H, Birouk M. Effect of swirl ratio on NG/diesel dual-fuel combustion at low to high engine load conditions. Appl Energ 2018;229:375-88.
[53] Shu J, Fu J, Liu J, Ma Y, Wang S, Deng B, et al. Effects of injector spray angle on combustion and emissions characteristics of a natural gas (NG)-diesel dual fuel engine based on CFD coupled with reduced chemical kinetic model. Appl Energ 2019;233-234:182-95.
[54] Shi C, Ji C, Wang S, Yang J, Li X, Ge Y. Effects of hydrogen direct-injection angle and charge concentration on gasoline-hydrogen blending lean combustion in a Wankel engine. Energ Convers Manage 2019;187:316-27.
[55] Zhou J, Sheng X, He L. Numerical Investigation of the Effect of Hydrogen Enrichment on an Opposed-Piston Compression Ignition Diesel Engine. Journal of Thermal Science 2019;28(4):669-81.
[56] Senecal PK, Pomraning E, Richards KJ, Briggs TE, Choi CY, McDavid RM, et al. Multi-Dimensional Modeling of Direct-Injection Diesel Spray Liquid Length and Flame Lift-off Length using CFD and Parallel Detailed Chemistry. SAE International; 2003.
[57] Bajaj C, Abraham J, Pickett LM. The role of vaporization in determining transient diesel spray structure. *23rd ILASS Americas.* 2011.
[58] Idicheria CA, Pickett LM. Quantitative mixing measurements in a vaporizing diesel spray by Rayleigh imaging. SAE Transactions 2007:490-504.
[59] Heywood JB. Internal combustion engine fundamentals. New York: McGraw-Hill; 1988.

[60] Rahimi A, Fatehifar E, Saray RK. Development of an optimized chemical kinetic mechanism for homogeneous charge compression ignition combustion of a fuel blend of n-heptane and natural gas using a genetic algorithm. Proceedings of the Institution of Mechanical Engineers, Part D: Journal of Automobile Engineering 2010;224(9):1141-59.

[61] Abidin Z, Florea R, Callahan T. Dual Fuel Combustion Study Using 3D CFD Tool. SAE International; 2016.

[62] Sun X, Liang X, Shu G, Lin J, Wang Y, Wang Y. Numerical investigation of two-stroke marine diesel engine emissions using exhaust gas recirculation at different injection time. Ocean Eng 2017;144:90-7.

[63] Shi C, Ji C, Ge Y, Wang S, Bao J, Yang J. Numerical study on ignition amelioration of a hydrogen-enriched Wankel engine under lean-burn condition. Appl Energ 2019;255:113800.

[64] Chen H, Reuss DL, Sick V. Analysis of misfires in a direct injection engine using proper orthogonal decomposition. Experiments in Fluids 2011;51(4):1139.

[65] Chen H, Xu M, Hung DLS, Zhuang H. Cycle-to-cycle variation analysis of early flame propagation in engine cylinder using proper orthogonal decomposition. Experimental Thermal and Fluid Science 2014;58:48-55.

[66] Rakopoulos CD, Rakopoulos DC, Mavropoulos GC, Kosmadakis GM. Investigating the EGR rate and temperature impact on diesel engine combustion and emissions under various injection timings and loads by comprehensive two-zone modeling. Energy 2018;157:990-1014.